Digital Signal Processing 86 (2019) 42–54

Contents lists available at ScienceDirect

Digital Signal Processing

www.elsevier.com/locate/dsp

Forward and backward extended Prony method for complex exponential signals with/without additive noise

Shuang Zhao *, Kenneth A. Loparo

Electrical Engineering and Computer Science Department, Case Western Reserve University, Cleveland, OH 44106, USA

ARTICLE INFO

Article history:
Available online 4 January 2019

Keywords:
Backward linear prediction
Complex exponentials
Forward linear prediction
Prony

ABSTRACT

We introduce a new strategy for finding the pole locations of signals composed of complex exponentials, and incorporate this strategy into the "Forward and Backward Extended Prony" (FBEP) method. The performance of the proposed method is investigated using statistical analysis and simulation experiments. Initial validation is accomplished using time-series data without additive noise, and the advantages of this method in accurately identifying both growing and decaying modes in moderate noise is then demonstrated by adding noise to the time-series data with different signal-to-noise ratios (SNRs). The FBEP method is compared with the TLS-Prony method and subspace-based methods by determining the mean squared errors (MSEs) of the frequency and damping factor estimates given by each method with comparing these to the corresponding Cramer–Rao (CR) bounds for white Gaussian noise cases. The FBEP method is also compared with a recent optimization-based iterative algorithm. The performance of the FBEP method using the pseudoinverse and Total Least Squares (TLS) approaches for different SNR is also studied. Previous polynomial methods are considered to be inferior to subspace-based methods (e.g., MODE, ESPRIT and Matrix Pencil) due to poor estimation accuracy under noise. As a polynomial method the FBEP method provides better performance than the MODE algorithm and comparable performance to the subspace-based methods that are well known for their accuracy and efficiency.

1. Introduction

Complex exponential signals are commonly encountered signals in a variety of systems and identifying the signal parameters is critical to studying several aspects of the system including stability and controller design. Prony methods, a type of linear parameter estimation method, have been developed and studied in numerous papers with applications to many fields including power systems [1,2], system identification and controller design [3,4], spectral estimation [5,6], biomedical engineering [7,8], speech signal processing [9], and radar and sonar systems [10,11]. Prony methods provide accurate results in identifying the modes of complex exponential signals in noise-free data regardless of the sign of the damping factors, however the original Prony method is sensitive to noise, and the estimation results from the extended Prony method also deviate significantly from the true parameter values with low signal-to-noise ratio (SNR) [12]. Many ideas have been proposed to improve the accuracy of Prony methods when noise is present. One class of methods optimizes the sampling interval and/or window size for Prony analysis, with optimal results when some index, e.g., the condition number, is minimum [13–16]. Another class of methods involves filtering the time-series data prior to or after Prony analysis. The filter may have constant coefficients [17] or include adaptation depending on the data [18–20].

The most effective and efficient modification to the Prony method uses singular value decomposition (SVD along with a high prediction order. Tufts and Kumaresan found that improved frequency estimation of undamped complex exponentials in noise can be obtained by increasing the order of the prediction error filter to be considerably larger than the actual number of modes in combination with SVD to reduce the impact of the noise [21]. These two techniques can also improve parameter estimation of "damped complex exponentials" corrupted by noise with low SNR by using an ingenious method for finding the true poles proposed by Kumaresan and Tufts [22]. In this method, complex conjugate data points are used to form a set of backward linear prediction equations and the boundary of the unit circle is used to help identify the signal zeros that are reflected inside the unit circle to estimate the true poles. This method implicitly constrains the signal so that the true poles are either on the boundary or inside the unit circle. Hence the method cannot be used to identify growing complex exponentials in the signal because the corresponding signal zeros

* Corresponding author.
E-mail addresses: sxz119@case.edu (S. Zhao), kenneth.loparo@case.edu (K.A. Loparo).

https://doi.org/10.1016/j.dsp.2018.12.012
1051-2004/

would be reflected inside the unit circle making it impossible to distinguish them from the extraneous zeros.

There are many important practical applications where decaying modes, undamped modes and growing (unstable) modes exist simultaneously in noisy measurements of complex exponential signals. For instance both stable and unstable as well as marginally stable modes may arise in power system low-frequency oscillations [23–25] and in radar scattering analysis where the modes in the radar cross section measurements may have arbitrary damping representing the degrees of concentration in the range of scattering centers [26]. Several methods use a higher prediction order to perform Prony analysis and then select the true modes iteratively by adding or removing the modes to approximate the actual signal according to some statistical criterion, for instance, residual sum of squares (RSS) [27], Akaike Information Criterion (AIC) [28] and the t-test [29].

Except Kumaresan and Tufts' method, all of the other above-mentioned methods contain iterative procedures either in the estimation process or in the separation of the true modes from the artificial modes, which results in increased computations and longer processing time. The TLS-Prony method is shown to be able to identify both damped/undamped and growing modes in a non-iterative way by retaining p (number of modes contained in the signal) poles with the highest energies [30]. Besides Prony, which is essentially a linear prediction (or polynomial) method, there are subspace-based estimation approaches for estimating complex exponentials with arbitrary damping factors, such as TLS Matrix Pencil (TLS-MP) [31], TLS-ESPRIT [32] and the MODE algorithm [33]. It is shown experimentally that the MODE algorithm performs better than the TLS-Prony method in the sense that the mean squared errors (MSEs) given by the MODE algorithm are closer to the Cramer–Rao (CR) bounds than those given by the TLS-Prony method. ESPRIT and Matrix Pencil are non-iterative methods that use SVD and are well known for their estimation accuracy and computational efficiency. Although they originate from different approaches, there is a connection between ESPRIT, Matrix Pencil and Prony methods [34]. Nonlinear methods can also be employed to estimate the parameters of complex exponentials by solving nonlinear optimization problems iteratively. For example, the SEMA algorithm gives frequency and damping factor estimates by iteratively solving optimization problems and updating the dictionary elements as well as creating a finer frequency grid. Although the adaptive dictionary learning approach mitigates the problem of having a large dictionary set when using other sparse reconstruction techniques, in each iteration several optimization problems have to be solved (where the number is determined by the number of amplitude peaks that are obtained as the solution of an optimization problem) and the entire process is repeated for each iteration with a refined frequency grid [35]. The ADMMHankel method iteratively solves a nonlinear least squares problem with a rank constraint on the Hankel matrix, and SVD is used in each step to find the low rank approximation of the Hankel matrix and the data sequence to generate the updated Hankel matrix is provided by solving a least squares problem. ESPRIT is eventually used to obtain the parameter estimates for the equally-spaced data case. The convergence to a global minimum is not guaranteed due to the non-convexity of the problem [36].

In light of practical needs in real-world applications, a good parameter estimation method should be able to identify the complex exponentials with arbitrary damping factors and provide accurate parameter estimation in substantial noise, with computational simplicity to be feasibly implemented in real-time. In this paper we propose the Forward and Backward Extended Prony (FBEP) method that gives accurate parameter estimation of decaying, undamped and growing complex exponential modes under moderately low SNRs. The FBEP method is based on a new pole identification strategy, which is shown in Section 2 for the noise-free case and benefits from the insight of Kumaresan on the properties of zeros of the linear prediction error filter given in [37]. Statistical analysis based on a first-order perturbation under high SNR is given in Section 3. In Section 4 the experimental performance of the FBEP method is investigated and compared with other methods that are able to identify both decaying and growing modes simultaneously. We draw conclusions in Section 5. Appendix A provides a comparison of the ADMMHankel optimization-based method [36] with the FBEP and TLS-ESPRIT methods and Appendix B shows the performance of FBEP and TLS-ESPRIT under pink noise. This paper focuses on the theoretical derivation and statistical analysis of the FBEP method with simulation results on a generic signal. Application of the FBEP method to power system small-signal stability analysis is given in [38].

2. The FBEP method

Consider a signal $x(t)$, which is the sum of complex exponentials and is uniformly sampled at time interval Δt to give a sampled data sequence in the form

$$x(n) = \sum_{i=1}^{p} b_i z_i^n, \quad n = 0, 1, \ldots, N-1 \tag{1}$$

with $b_i = A_i \exp[j\theta_i]$ and $z_i = \exp[(d_i + j2\pi f_i)\Delta t]$, and p is the number of complex exponentials. The poles are assumed to be distinct and nonzero. The residues include the amplitudes A_i and phases θ_i, and the frequencies f_i and damping factors d_i can be obtained from the poles. Let

$$H(z) = \sum_{k=0}^{P_e} h_k z^{-k}, \quad h_0 = 1 \tag{2}$$

denote the general form of a monic polynomial of order P_e with coefficient vector $\mathbf{h} = [1, h_1, \cdots, h_{P_e}]^T$.

Proposition 1. *If $p \le P_e \le N - p$ and $\mathbf{h}$ is the solution vector of a set of forward linear prediction equations (3), then $H(z)$ has zeros at z_i, $i = 1, 2, \ldots, p$.*

$$\begin{bmatrix} x(P_e) & x(P_e-1) & \cdots & x(0) \\ x(P_e+1) & x(P_e) & \cdots & x(1) \\ \vdots & \vdots & \ddots & \vdots \\ x(N-1) & x(N-2) & \cdots & x(N-P_e-1) \end{bmatrix} \begin{bmatrix} 1 \\ h_1 \\ \vdots \\ h_{P_e} \end{bmatrix} = 0 \tag{3}$$

This proposition was originally proved by Kumaresan in [37], and will be used in our new pole identification strategy shown later. The set of forward linear prediction equations can be written as

$$\sum_{k=0}^{P_e} h_k x(n-k) = 0, \quad P_e \le n \le N-1 \tag{4}$$

where $h_0 = 1$ and $p \le P_e \le N - p$ and the polynomial $H(z) = \sum_{k=0}^{P_e} h_k z^{-k}$ has zeros at $z_i, i = 1, 2, \ldots, p$.

Proposition 2. *If $p \le P_e \le N - p$ and $\mathbf{h}$ is the solution vector of a set of backward linear prediction equations (5), then $H(z)$ has zeros at $1/z_i, i = 1, 2, \ldots, p$.*

$$\begin{bmatrix} x(0) & x(1) & \cdots & x(P_e) \\ x(1) & x(2) & \cdots & x(P_e+1) \\ \vdots & \vdots & \ddots & \vdots \\ x(N-P_e-1) & x(N-P_e) & \cdots & x(N-1) \end{bmatrix} \begin{bmatrix} 1 \\ h_1 \\ \vdots \\ h_{P_e} \end{bmatrix} = 0 \tag{5}$$

Proof. The set of backward linear prediction equations can be written as

$$\sum_{k=0}^{P_e} h_k x(n+k) = 0, \quad 0 \le n \le N-1-P_e \tag{6}$$

where $h_0 = 1$ and $p \le P_e \le N-p$. Substitute (1) into the above equation,

$$\sum_{k=0}^{P_e} h_k x(n+k) = \sum_{k=0}^{P_e} h_k \sum_{i=1}^{p} b_i z_i^{n+k} = \sum_{i=1}^{p} b_i z_i^n \sum_{k=0}^{P_e} h_k z_i^k = 0 \tag{7}$$

For (7) to hold, the coefficients of the p linearly independent vectors $\{b_1 z_1^n\}, \{b_2 z_2^n\}, \cdots, \{b_p z_p^n\}, (0 \le n \le N-1-P_e)$ must all be zero, i.e.,

$$\sum_{k=0}^{P_e} h_k z_i^k = 0, \quad i = 1, 2, \ldots, p \tag{8}$$

Hence the polynomial $H(z) = \sum_{k=0}^{P_e} h_k z^{-k}$ has zeros at $1/z_i$, $i = 1, 2, \ldots, p$. The constraint on P_e is due to the fact that the rank of the backward data matrix in (5) is p, so at least p equations are required. In addition we are seeking at least one solution so the dimension of the null space of the matrix must be no less than one, hence we have $p \le P_e \le N-p$.

Next we present the notation that will be in the propositions that follow. $\mathbf{h}^f$ and $\mathbf{h}^b$ are minimum norm solution vectors of (3) and (5) respectively with $H^f(z)$ and $H^b(z)$ the corresponding monic polynomials of order P_e with signal zeros (related to the true poles) and extraneous zeros (due to overestimating the linear prediction order).

Proposition 3. *The $P_e - p$ extraneous zeros of $H^f(z)$ and $H^b(z)$ are inside the unit circle. Moreover the extraneous zeros of $H^b(z)$ are complex conjugates of those of $H^f(z)$.*

Proof. Factor $H(z)$ into two monic polynomials $H_1(z)$ and $H_2(z)$

$$H_1(z) = 1 + l_1 z^{-1} + l_2 z^{-2} + \cdots + l_p z^{-p} \tag{9}$$

$$H_2(z) = 1 + c_1 z^{-1} + c_2 z^{-2} + \cdots + c_{P_e-p} z^{-(P_e-p)} \tag{10}$$

where $H_1(z)$ is a pth order polynomial formed by the signal zeros, and $H_2(z)$ is a $(P_e - p)$th order polynomial formed by the extraneous zeros. The coefficient h_n is obtained by convolving the sequences l_n and c_n, i.e.,

$$h_n = \sum_{k=-\infty}^{\infty} c_{n-k} l_k \tag{11}$$

where $h_0 = c_0 = l_0 = 1, c_k = 0$ if $k < 0$ or $k > P_e - p$ and $l_k = 0$ if $k < 0$ or $k > p$. If we view $1, l_1, \cdots, l_p$ as a "data sequence" passing through a linear prediction error filter $H_2(z)$ with coefficients $1, c_1, \cdots, c_{P_e-p}$ as given in (10), then the sequence $1, h_1, \cdots, h_{P_e}$ is the output "error sequence". The coefficients of $H_2(z)$ that minimize the norm of the output error sequence are found by solving the normal equations given by the autocorrelation method. These normal equations, equivalent to the Yule–Walker equations [12], are given in (12).

$$\begin{bmatrix} R(0) & R(-1) & \cdots & R(1-P_e+p) \\ R(1) & R(0) & \cdots & R(2-P_e+p) \\ \vdots & \vdots & \ddots & \vdots \\ R(P_e-p-1) & R(P_e-p-2) & \cdots & R(0) \end{bmatrix} \times \begin{bmatrix} c_1 \\ c_2 \\ \vdots \\ c_{P_e-p} \end{bmatrix} = - \begin{bmatrix} R(1) \\ R(2) \\ \vdots \\ R(P_e-p) \end{bmatrix} \tag{12}$$

where

$$R(j) = \sum_{m=0}^{p} l_m^* l_{m+j} \tag{13}$$

It is well-known that the solution of the Yule–Walker equations is a stable filter whose zeros are inside the unit circle [39]. Therefore the zeros of $H_2(z)$, equivalently the extraneous zeros of $H(z)$ are inside the unit circle. Recall that $H(z)$ is a monic polynomial of order P_e similar to $H^f(z)$ and $H^b(z)$, hence the extraneous zeros of both $H^f(z)$ and $H^b(z)$ are inside the unit circle.

Denote the signal zero polynomials of $H^f(z)$ and $H^b(z)$ as $H_1^f(z)$ and $H_1^b(z)$, and the extraneous zero polynomials as $H_2^f(z)$ and $H_2^b(z)$, respectively. The zeros of $H_1^b(z)$ are reciprocals of those of $H_1^f(z)$ according to Propositions 1 and 2, and the coefficients of $H_1^b(z)$ are the same as those of $H_1^f(z)$ but in reverse order and scaled by a constant; that is, if the coefficients of $H_1^f(z)$ are $1, l_1, \cdots, l_p$, then the coefficients of $H_1^b(z)$ are $(l_p, l_{p-1}, \cdots, 1)/l_p$. Therefore, the autocorrelation terms $R(j)$ in (13) are changed to their complex conjugates and the same scaling is applied to each term on both sides of (12). The coefficients of $H_2^b(z)$ are complex conjugates of those of $H_2^f(z)$, so that the zeros of $H_2^b(z)$ are complex conjugates of those of $H_2^f(z)$. This completes the proof of Proposition 3.

Proposition 4. *If $\mathbf{h}^r = [h_{P_e}, h_{P_e-1}, \cdots, h_1, 1]^T$ is the minimum norm solution vector of (14) where $p \le P_e \le N-p$, then $H^r(z) = h_{P_e} + h_{P_e-1} z^{-1} + \cdots + h_1 z^{-(P_e-1)} + z^{-P_e}$ has zeros at $z_i, i = 1, 2, \ldots, p$ with extraneous zeros outside the unit circle. The extraneous zeros are complex conjugate reciprocals of the zeros of $H^f(z)$ whose coefficient vector $\mathbf{h}^f$ is the minimum norm solution of (3).*

$$\begin{bmatrix} x(P_e) & x(P_e-1) & \cdots & x(0) \\ x(P_e+1) & x(P_e) & \cdots & x(1) \\ \vdots & \vdots & \ddots & \vdots \\ x(N-1) & x(N-2) & \cdots & x(N-P_e-1) \end{bmatrix} \begin{bmatrix} h_{P_e} \\ \vdots \\ h_1 \\ 1 \end{bmatrix} = 0 \tag{14}$$

Proof. The set of backward linear prediction equations (5) with minimum norm solution $\mathbf{h}^b$ can also be written by reversing the order of the matrix columns and the elements of $\mathbf{h}^b$ simultaneously, as shown in (14). Hence $\mathbf{h}^r$ is $\mathbf{h}^b$ in reverse order. Therefore, the zeros of $H^r(z)$, including both signal and extraneous zeros, are reciprocals of the zeros of $H^b(z)$. From Propositions 1, 2, and 3, it is clear that $H^r(z)$ has zeros at $z_i, i = 1, 2, \ldots, p$, with extraneous zeros that are complex conjugate reciprocals of the zeros of $H^f(z)$. According to Proposition 3, the extraneous zeros of $H^f(z)$ are inside the unit circle, and thus the extraneous zeros of $H^r(z)$ are outside the unit circle. The constraint on the prediction order is given for the same reason as in the proof of Proposition 2. The proof is complete.

Proposition 5. *If the prediction order P_e is chosen to be equal to p which is the actual number of complex exponentials in the signal with $\mathbf{h}_p^f = [1, h_1^f, \cdots, h_p^f]^T$ and $\mathbf{h}_p^r = [h_p^r, h_{p-1}^r, \cdots, h_1^r, 1]^T$ the minimum norm solution vectors of (3) and (14) respectively, then $\mathbf{h}_p^r$ is a scaled version of $\mathbf{h}_p^f$ given by:*

$$\left[h_p^r, h_{p-1}^r, \cdots, h_1^r, 1\right]^T = \left[1, h_1^f, \cdots, h_p^f\right]^T / h_p^f \tag{15}$$

Proof. Follows directly from Propositions 1 and 4 with the following observations: the signal zeros $z_i, i = 1, 2, \ldots, p$ are the same for the polynomials $H_p^f(z) = 1 + h_1^f z^{-1} + \cdots + h_p^f z^{-p}$ and $H_p^r(z) = h_p^r + h_{p-1}^r z^{-1} + \cdots + h_1^r z^{-(p-1)} + z^{-p}$ and with P_e equal to p, there are no extraneous zeros and thus $\mathbf{h}_p^r$ is obtained by dividing $\mathbf{h}_p^f$ by its last element so that the last element in $\mathbf{h}_p^r$ is equal to one. The proof is complete.

From Propositions 1, 3 and 4 we observe that the forward characteristic polynomial $H^f(z)$ has signal zeros at the true poles $z_i, i = 1, 2, \ldots, p$, with the extraneous zeros located inside the unit circle. The backward characteristic polynomial $H^r(z)$ has the same signal zeros with the extraneous zeros located outside the unit circle. Based on this property, we develop a new strategy to find the true poles: 1) calculate the minimum norm solutions $\mathbf{h}^f$ and $\mathbf{h}^r$ by solving (3) and (14) to obtain the corresponding forward and backward characteristic polynomials $H^f(z)$ and $H^r(z)$; 2) collect the zeros of $H^r(z)$ inside the unit circle (these are the poles of the decaying modes) and the zeros of $H^f(z)$ outside the unit circle (these are the poles of the growing modes). If there are zeros on the unit circle (these are the poles of undamped modes) they can be collected from either the forward or backward characteristic polynomials. By combining these two sets of zeros, all true poles are obtained. Because (3) and (14) have the same data matrix, we can obtain the coefficients of both the forward and backward characteristic polynomials by constructing only one data matrix.

When additive white Gaussian noise is present, depending on the actual SNR, the above property still holds if we use SVD to obtain a low rank approximation of the data matrix, along with the Total Least Squares (TLS) [40] or pseudoinverse method to find the minimum norm solutions of the relevant equations. The TLS method gives better results than the pseudoinverse method with low SNR because it considers the errors in the observation vector and in the data matrix. Another advantage of the TLS approach is that we can obtain both forward and backward characteristic polynomial coefficients with a single SVD applied to the data matrix. In practical cases the number of complex exponentials contained in the signal, if unknown, can be estimated by the effective rank [41] that is then used to obtain the low rank approximation. By incorporating our strategy into the Extended Prony method, we can successfully identify all parameters of complex exponential signals with moderate SNR regardless of the sign of the damping factor. We refer to this method as the "Forward and Backward Extended Prony" (FBEP) method. The steps in the method are summarized as follows [38,42]:

1. Construct the data matrix in (16) with prediction order P_e satisfying $p \le P_e \le N - p$, where p is the number complex exponentials contained in $x(n)$ of length N.

$$\mathbf{X} = \begin{bmatrix} x(P_e) & x(P_e - 1) & \cdots & x(0) \\ x(P_e + 1) & x(P_e) & \cdots & x(1) \\ \vdots & \vdots & \ddots & \vdots \\ x(N-1) & x(N-2) & \cdots & x(N - P_e - 1) \end{bmatrix} \tag{16}$$

2. Use the Pseudoinverse or Total Lease Squares (TLS) method to find two minimum norm solution vectors in the null space of $\mathbf{X}$: $\mathbf{h}^f = [1, h_1^f, \cdots, h_{P_e}^f]^T$ and $\mathbf{h}^r = [h_{P_e}^r, h_{P_e-1}^r, \cdots, h_1^r, 1]^T$.
3. Construct the forward characteristic polynomial $H^f(z) = 1 + h_1^f z^{-1} + \cdots + h_{P_e}^f z^{-P_e}$ and the backward characteristic polynomial $H^r(z) = h_{P_e}^r + h_{P_e-1}^r z^{-1} + \cdots + h_1^r z^{-(P_e-1)} + z^{-P_e}$ respectively. Collect the zeros of $H^r(z)$ inside the unit circle and the zeros of $H^f(z)$ outside the unit circle. If there are zeros on the unit circle, they can be collected from either the forward or backward characteristic polynomials. Combine these two sets of zeros to obtain all the true poles $z_i, i = 1, 2, \cdots, p$.
4. Compute the residues $b_i, i = 1, 2, \cdots, p$ by solving

$$\begin{bmatrix} 1 & 1 & \cdots & 1 \\ z_1 & z_2 & \cdots & z_p \\ \vdots & \vdots & \vdots & \vdots \\ z_1^{N-1} & z_2^{N-1} & \cdots & z_p^{N-1} \end{bmatrix} \begin{bmatrix} b_1 \\ b_2 \\ \vdots \\ b_p \end{bmatrix} = \begin{bmatrix} x(0) \\ x(1) \\ \vdots \\ x(N-1) \end{bmatrix} \tag{17}$$

5. The amplitudes A_i, frequencies f_i, damping factors d_i and phases θ_i are given by

$$\begin{cases} f_i = \arctan(Im(z_i)/\operatorname{Re}(z_i))/(2\pi\,\Delta t) \\ d_i = \ln|z_i|/\Delta t \\ A_i = |b_i| \\ \theta_i = \arctan(Im(b_i)/\operatorname{Re}(b_i)), \end{cases} \quad 1 \le i \le p \tag{18}$$

If the data sequence $x(n)$ is contaminated by additive white Gaussian noise, replace the data points in (16) and (17) by the noisy data points and a low-rank approximation is performed using the largest p singular values and their corresponding singular vectors when solving for the minimum norm solutions in step 2.

3. Statistical analysis of FBEP

Suppose that the data sequence given in (1) is measured in additive noise with

$$y(n) = x(n) + e(n), \quad n = 0, 1, \ldots, N-1 \tag{19}$$

where $e(n)$ is zero-mean complex-valued white Gaussian noise with uncorrelated real and imaginary parts where each part has variance σ^2. Denote the mode parameter vector $\boldsymbol{\eta} = [\mathbf{f}^T \;\; \mathbf{f}_r^T \;\; \mathbf{d}^T \;\; \mathbf{d}_r^T]^T$ where $\mathbf{f}$ and $\mathbf{d}$ are vectors of frequencies and damping factors of growing modes, with the parameters of the decaying modes given in $\mathbf{f}_r$ and $\mathbf{d}_r$, respectively. The corresponding parameters of the undamped modes can be included in either of the two sets of parameters.

Theorem. *Define the FBEP estimate* $\hat{\boldsymbol{\eta}} = [\hat{\mathbf{f}}^T \;\; \hat{\mathbf{f}}_r^T \;\; \hat{\mathbf{d}}^T \;\; \hat{\mathbf{d}}_r^T]^T$, *then to a first-order approximation (as* $\sigma^2 \to 0$*)* $\hat{\boldsymbol{\eta}}$ *has a normal distribution*

$$\hat{\boldsymbol{\eta}} \sim N(\boldsymbol{\eta}, \Sigma_{\hat{\eta}}) \tag{20}$$

where

$$\Sigma_{\hat{\eta}} = \begin{bmatrix} \frac{\sigma^2}{(2\pi\Delta t)^2}\operatorname{Re}\{\mathbf{QQ}^H\} & \frac{-\sigma^2}{(2\pi\Delta t)^2}\operatorname{Re}\{\mathbf{QS}^H\} & \frac{\sigma^2}{2\pi\Delta t^2}\operatorname{Im}\{\mathbf{QQ}^H\} & \frac{-\sigma^2}{2\pi\Delta t^2}\operatorname{Im}\{\mathbf{QS}^H\} \\ \frac{-\sigma^2}{(2\pi\Delta t)^2}\operatorname{Re}\{\mathbf{SQ}^H\} & \frac{\sigma^2}{(2\pi\Delta t)^2}\operatorname{Re}\{\mathbf{SS}^H\} & \frac{-\sigma^2}{2\pi\Delta t^2}\operatorname{Im}\{\mathbf{SQ}^H\} & \frac{\sigma^2}{2\pi\Delta t^2}\operatorname{Im}\{\mathbf{SS}^H\} \\ \frac{\sigma^2}{2\pi\Delta t^2}\operatorname{Im}\{\mathbf{QQ}^H\} & \frac{-\sigma^2}{2\pi\Delta t^2}\operatorname{Im}\{\mathbf{QS}^H\} & \frac{\sigma^2}{\Delta t^2}\operatorname{Re}\{\mathbf{QQ}^H\} & \frac{-\sigma^2}{\Delta t^2}\operatorname{Re}\{\mathbf{QS}^H\} \\ \frac{-\sigma^2}{2\pi\Delta t^2}\operatorname{Im}\{\mathbf{SQ}^H\} & \frac{\sigma^2}{2\pi\Delta t^2}\operatorname{Im}\{\mathbf{SS}^H\} & \frac{-\sigma^2}{\Delta t^2}\operatorname{Re}\{\mathbf{SQ}^H\} & \frac{\sigma^2}{\Delta t^2}\operatorname{Re}\{\mathbf{SS}^H\} \end{bmatrix} \tag{21}$$

The expressions for $\mathbf{Q}$ and $\mathbf{S}$ are derived in the Proof. $\mathbf{QQ}^H$ and $\mathbf{SS}^H$ are Hermitian matrices with real-valued diagonal elements, $\operatorname{cov}(\hat{f}_i, \hat{d}_i) = 0$ and $\operatorname{cov}(\hat{f}_{ri}, \hat{d}_{ri}) = 0$, so the frequency and damping factor estimates of the same mode are uncorrelated and independent. The variance of the frequency estimate is $1/4\pi^2$ times the variance of the damping factor estimate for each mode indicating that the damping factors are more sensitive to noise than the frequency estimates. If the angular frequency $(2\pi\mathbf{f}, 2\pi\mathbf{f}_r)$ is considered instead, the $1/4\pi^2$ scaling disappears so that the noise has equal influence on the damping factor and angular frequency estimates.

Proof. The forward linear prediction data matrix formed by the noisy data sequence can be written as

$$\left[\,\mathbf{y}\,|\,\mathbf{Y}\,\right]=\left[\,\mathbf{x}\,|\,\mathbf{X}\,\right]+\left[\,\mathbf{n}\,|\,\mathbf{N}\,\right] \tag{22}$$

where $[\mathbf{x}\,|\,\mathbf{X}]$ is the noiseless data matrix of the forward linear prediction equations

$$\left[\,\mathbf{x}\,|\,\mathbf{X}\,\right]\begin{bmatrix}1\\ \mathbf{g}\end{bmatrix}=\mathbf{0} \tag{23}$$

with

$$\begin{aligned}\mathbf{x}&=\begin{bmatrix}x(P_e) & x(P_e+1) & \cdots & x(N-1)\end{bmatrix}^T\\ \mathbf{X}&=\begin{bmatrix}x(P_e-1) & x(P_e-2) & \cdots & x(0)\\ x(P_e) & x(P_e-1) & \cdots & x(1)\\ \vdots & \vdots & \ddots & \vdots\\ x(N-2) & x(N-3) & \cdots & x(N-P_e-1)\end{bmatrix}\\ \mathbf{g}&=\begin{bmatrix}g_1 & g_2 & \cdots & g_{P_e}\end{bmatrix}^T\end{aligned} \tag{24}$$

Suppose $[\mathbf{y}_T\,|\,\mathbf{Y}_T]$ is the rank-p low rank approximation of $[\mathbf{y}\,|\,\mathbf{Y}]$, then the FBEP solves for the equation

$$\left[\,\mathbf{y}_T\,|\,\mathbf{Y}_T\,\right]\begin{bmatrix}1\\ \hat{\mathbf{g}}\end{bmatrix}=\mathbf{0} \tag{25}$$

Let $[\mathbf{y}_T\,|\,\mathbf{Y}_T]=[\mathbf{x}\,|\,\mathbf{X}]+[\Delta\mathbf{x}\,|\,\Delta\mathbf{X}]$ with $\hat{\mathbf{g}}=\mathbf{g}+\Delta\mathbf{g}$, where the quantities preceded by Δ represent the case with small perturbations due to noise. The following relationship can be readily obtained [43]

$$\mathbf{X}\Delta\mathbf{g}=-\mathbf{X}\mathbf{X}^{+}\boldsymbol{\varepsilon} \tag{26}$$

where $\boldsymbol{\varepsilon}=\mathbf{n}+\mathbf{N}\mathbf{g}$. Note that $\mathbf{X}=\mathbf{H}\mathbf{G}$ with

$$\begin{aligned}\mathbf{H}&=\begin{bmatrix}b_1z_1^{P_e} & b_2z_2^{P_e} & \cdots & b_pz_p^{P_e}\\ b_1z_1^{P_e+1} & b_2z_2^{P_e+1} & \cdots & b_pz_p^{P_e+1}\\ \vdots & \vdots & \ddots & \vdots\\ b_1z_1^{N-1} & b_2z_2^{N-1} & \cdots & b_pz_p^{N-1}\end{bmatrix}\\ \mathbf{G}&=\begin{bmatrix}z_1^{-1} & z_1^{-2} & \cdots & z_1^{-P_e}\\ z_2^{-1} & z_2^{-2} & \cdots & z_2^{-P_e}\\ \vdots & \vdots & \vdots & \vdots\\ z_p^{-1} & z_p^{-2} & \cdots & z_p^{-P_e}\end{bmatrix}\end{aligned} \tag{27}$$

Because $\mathbf{H}$ is of full column rank and $\mathbf{G}$ is of full row rank, (26) is equivalent to

$$\mathbf{G}\Delta\mathbf{g}=-\mathbf{H}^{+}\boldsymbol{\varepsilon} \tag{28}$$

Performing a first-order Taylor series expansion on the forward characteristic equation

$$1+\sum_{k=1}^{P_e}\hat{g}_k\hat{z}_i^{-k}=0 \tag{29}$$

leads to

$$\Delta z_i=\frac{\sum_{k=1}^{P_e}\Delta g_k z_i^{-k}}{\sum_{k=1}^{P_e}kg_kz_i^{-(k+1)}} \tag{30}$$

Suppose $z_1, z_2\cdots, z_m$ are m poles with nonnegative damping factors, and $z_{m+1}, z_{m+2}, \cdots z_p$ are poles with negative damping factors, let $\zeta_i=\sum_{k=1}^{P_e}kg_kz_i^{-(k+1)}$, we have

$$\Delta\mathbf{Z}=\mathbf{F}\mathbf{D}\mathbf{G}\Delta\mathbf{g} \tag{31}$$

where $\Delta\mathbf{Z}=[\Delta z_1, \Delta z_2, \cdots, \Delta z_m]^T$, $\mathbf{F}$ is a m-by-m diagonal matrix with $1/\zeta_i, i=1,2,\ldots,m$ as the diagonal elements and $\mathbf{D}$ is a m-by-p matrix with ones on the diagonal of a m-by-m submatrix and zeros elsewhere, i.e.,

$$\begin{aligned}\mathbf{F}&=diag(1/\zeta_1, 1/\zeta_2, \cdots, 1/\zeta_m)\\ \mathbf{D}&=\begin{bmatrix}1 & 0 & 0 & \cdots & 0 & 0 & 0\\ 0 & 1 & 0 & 0 & \cdots & 0 & 0\\ \vdots & \ddots & \ddots & \ddots & \ddots & \ddots & \vdots\\ 0 & \cdots & 0 & 1 & 0 & \cdots & 0\end{bmatrix}_{m\times p}\end{aligned} \tag{32}$$

Incorporating (28) into (31),

$$\Delta\mathbf{Z}=-\mathbf{F}\mathbf{D}\mathbf{H}^{+}\boldsymbol{\varepsilon} \tag{33}$$

Recall that $z_i=\exp[(d_i+j2\pi f_i)\Delta t]$, hence

$$\Delta z_i/z_i=\Delta t\Delta d_i+j2\pi\,\Delta t\Delta f_i \tag{34}$$

Therefore

$$\begin{aligned}\Delta\mathbf{f}&=\frac{1}{2\pi\,\Delta t}\,\mathrm{Im}\{\mathbf{T}\Delta\mathbf{Z}\}=\frac{1}{2\pi\,\Delta t}\,\mathrm{Im}\{-\mathbf{T}\mathbf{F}\mathbf{D}\mathbf{H}^{+}\boldsymbol{\varepsilon}\}\\ \Delta\mathbf{d}&=\frac{1}{\Delta t}\,\mathrm{Re}\{\mathbf{T}\Delta\mathbf{Z}\}=\frac{1}{\Delta t}\,\mathrm{Re}\{-\mathbf{T}\mathbf{F}\mathbf{D}\mathbf{H}^{+}\boldsymbol{\varepsilon}\}\end{aligned} \tag{35}$$

where $\mathbf{T}=diag(1/z_1, 1/z_2, \cdots, 1/z_m)$.

The covariance matrix of $\boldsymbol{\varepsilon}$ is given by

$$E\{\boldsymbol{\varepsilon}\boldsymbol{\varepsilon}^H\}=E\left\{\left(\left[\,\mathbf{n}\,|\,\mathbf{N}\,\right]\begin{bmatrix}1\\ \mathbf{g}\end{bmatrix}\right)\left(\left[\,\mathbf{n}\,|\,\mathbf{N}\,\right]\begin{bmatrix}1\\ \mathbf{g}\end{bmatrix}\right)^H\right\}=2\sigma^2\mathbf{P}\mathbf{P}^H \tag{36}$$

with

$$\mathbf{P}=\begin{bmatrix}g_{P_e} & g_{P_e-1} & \cdots & 1 & 0 & 0 & \cdots & 0\\ 0 & g_{P_e} & g_{P_e-1} & \cdots & 1 & 0 & \cdots & 0\\ \vdots & \vdots & \ddots & \ddots & & \ddots & \ddots & \vdots\\ 0 & 0 & \cdots & 0 & g_{P_e} & g_{P_e-1} & \cdots & 1\end{bmatrix}_{(N-P_e)\times N} \tag{37}$$

Use the following from [44]

$$\begin{aligned}\mathrm{Re}\{\mathbf{u}\}\,\mathrm{Re}\{\mathbf{v}^T\}&=\frac{1}{2}\left[\mathrm{Re}\{\mathbf{u}\mathbf{v}^T\}+\mathrm{Re}\{\mathbf{u}\mathbf{v}^H\}\right]\\ \mathrm{Im}\{\mathbf{u}\}\,\mathrm{Im}\{\mathbf{v}^T\}&=-\frac{1}{2}\left[\mathrm{Re}\{\mathbf{u}\mathbf{v}^T\}-\mathrm{Re}\{\mathbf{u}\mathbf{v}^H\}\right]\\ \mathrm{Im}\{\mathbf{u}\}\,\mathrm{Re}\{\mathbf{v}^T\}&=\frac{1}{2}\left[\mathrm{Im}\{\mathbf{u}\mathbf{v}^T\}+\mathrm{Im}\{\mathbf{u}\mathbf{v}^H\}\right]\end{aligned} \tag{38}$$

with the fact that $E\{\boldsymbol{\varepsilon}\boldsymbol{\varepsilon}^T\}=\mathbf{0}$, to obtain

$$\begin{aligned}E\{\Delta\mathbf{f}\Delta\mathbf{f}^T\}&=\frac{\sigma^2}{(2\pi\,\Delta t)^2}\,\mathrm{Re}\{\mathbf{Q}\mathbf{Q}^H\}\\ E\{\Delta\mathbf{d}\Delta\mathbf{d}^T\}&=\frac{\sigma^2}{\Delta t^2}\,\mathrm{Re}\{\mathbf{Q}\mathbf{Q}^H\}\\ E\{\Delta\mathbf{f}\Delta\mathbf{d}^T\}&=\frac{\sigma^2}{2\pi\,\Delta t^2}\,\mathrm{Im}\{\mathbf{Q}\mathbf{Q}^H\}\end{aligned} \tag{39}$$

where

$$\mathbf{Q} = \mathbf{TFDH}^{+}\mathbf{P} \tag{40}$$

Similarly the backward linear prediction equations formed by the noisy data sequence is

$$\left[\, \mathbf{Y}_r \mid \mathbf{y}_r \,\right] = \left[\, \mathbf{X}_r \mid \mathbf{x}_r \,\right] + \left[\, \mathbf{N}_r \mid \mathbf{n}_r \,\right] \tag{41}$$

where $[\mathbf{X}_r \mid \mathbf{x}_r]$ is the noiseless data matrix of the backward linear prediction equations

$$\left[\, \mathbf{X}_r \mid \mathbf{x}_r \,\right] \begin{bmatrix} \mathbf{g}^r \\ 1 \end{bmatrix} = \mathbf{0} \tag{42}$$

with the minimum solution $[(\mathbf{g}^r)^T \quad 1]^T$, and

$$\begin{aligned} \mathbf{x}_r &= \begin{bmatrix} x(0) & x(1) & \cdots & x(N-P_e-1) \end{bmatrix}^T \\ \mathbf{X}_r &= \begin{bmatrix} x(P_e) & x(P_e-1) & \cdots & x(1) \\ x(P_e+1) & x(P_e) & \cdots & x(2) \\ \vdots & \vdots & \ddots & \vdots \\ x(N-1) & x(N-2) & \cdots & x(N-P_e) \end{bmatrix} \\ \mathbf{g}^r &= \begin{bmatrix} g^r_{P_e} & \cdots & g^r_1 & 1 \end{bmatrix}^T \end{aligned} \tag{43}$$

Due to the fact that the poles are nonzero, the backward characteristic equation can be written as

$$1 + g^r_1 z + \cdots g^r_{P_e-1} z^{P_e-1} + g^r_{P_e} z^{P_e} = 0 \tag{44}$$

Note that $\mathbf{X}_r = \mathbf{H}_r\mathbf{G}_r$ with

$$\begin{aligned} \mathbf{H}_r &= \begin{bmatrix} b_1 z_1^0 & b_2 z_2^0 & \cdots & b_p z_p^0 \\ b_1 z_1^1 & b_2 z_2^1 & \cdots & b_p z_p^1 \\ \vdots & \vdots & \ddots & \vdots \\ b_1 z_1^{N-P_e-1} & b_2 z_2^{N-P_e-1} & \cdots & b_p z_p^{N-P_e-1} \end{bmatrix} \\ \mathbf{G}_r &= \begin{bmatrix} z_1^{P_e} & z_1^{P_e-1} & \cdots & z_1^1 \\ z_2^{P_e} & z_2^{P_e-1} & \cdots & z_2^1 \\ \vdots & \vdots & \vdots & \vdots \\ z_p^{P_e} & z_p^{P_e-1} & \cdots & z_p^1 \end{bmatrix} \end{aligned} \tag{45}$$

Define

$$\boldsymbol{\varepsilon}_r = \left[\, \mathbf{N}_r \mid \mathbf{n}_r \,\right] \begin{bmatrix} \mathbf{h}^r \\ 1 \end{bmatrix}, \qquad \beta_i = \sum_{k=1}^{P_e} k g^r_k z_i^{k-1} \tag{46}$$

Following similar procedures as in the forward linear prediction part we obtain

$$\begin{aligned} \Delta\mathbf{f}_r &= \frac{1}{2\pi\,\Delta t}\,\mathrm{Im}\{\mathbf{T}_r\mathbf{F}_r\mathbf{D}_r\mathbf{H}_r^{+}\boldsymbol{\varepsilon}_r\} \\ \Delta\mathbf{d}_r &= \frac{1}{\Delta t}\,\mathrm{Re}\{\mathbf{T}_r\mathbf{F}_r\mathbf{D}_r\mathbf{H}_r^{+}\boldsymbol{\varepsilon}_r\} \end{aligned} \tag{47}$$

hence

$$\begin{aligned} E\left\{\Delta\mathbf{f}_r\Delta\mathbf{f}_r^T\right\} &= \frac{\sigma^2}{(2\pi\,\Delta t)^2}\,\mathrm{Re}\left\{\mathbf{SS}^H\right\} \\ E\left\{\Delta\mathbf{d}_r\Delta\mathbf{d}_r^T\right\} &= \frac{\sigma^2}{\Delta t^2}\,\mathrm{Re}\left\{\mathbf{SS}^H\right\} \\ E\left\{\Delta\mathbf{f}_r\Delta\mathbf{d}_r^T\right\} &= \frac{\sigma^2}{2\pi\,\Delta t^2}\,\mathrm{Im}\left\{\mathbf{SS}^H\right\} \end{aligned} \tag{48}$$

and

$$\begin{aligned} E\left\{\Delta\mathbf{f}\Delta\mathbf{f}_r^T\right\} &= \frac{-\sigma^2}{(2\pi\,\Delta t)^2}\,\mathrm{Re}\left\{\mathbf{QS}^H\right\} \\ E\left\{\Delta\mathbf{d}\Delta\mathbf{d}_r^T\right\} &= \frac{-\sigma^2}{\Delta t^2}\,\mathrm{Re}\left\{\mathbf{QS}^H\right\} \\ E\left\{\Delta\mathbf{f}\Delta\mathbf{d}_r^T\right\} &= \frac{-\sigma^2}{2\pi\,\Delta t^2}\,\mathrm{Im}\left\{\mathbf{QS}^H\right\} \\ E\left\{\Delta\mathbf{f}_r\Delta\mathbf{d}^T\right\} &= \frac{-\sigma^2}{2\pi\,\Delta t^2}\,\mathrm{Im}\left\{\mathbf{SQ}^H\right\} \end{aligned} \tag{49}$$

where

$$\begin{aligned} \mathbf{S} &= \mathbf{T}_r\mathbf{F}_r\mathbf{D}_r\mathbf{H}_r^{+}\mathbf{P}_r \\ \mathbf{T}_r &= diag(1/z_{m+1}, 1/z_{m+2}, \cdots, 1/z_p) \\ \mathbf{F}_r &= diag(1/\beta_{m+1}, 1/\beta_{m+2}, \cdots, 1/\beta_p) \\ \mathbf{D}_r &= \begin{bmatrix} 0 & \cdots & 0 & 1 & 0 & 0 & 0 \\ 0 & 0 & \cdots & 0 & 1 & 0 & 0 \\ \vdots & \ddots & \ddots & \ddots & \ddots & \ddots & \vdots \\ 0 & \cdots & 0 & \cdots & 0 & 0 & 1 \end{bmatrix}_{(p-m)\times p} \end{aligned} \tag{50}$$

and

$$\mathbf{P}_r = \begin{bmatrix} 1 & g^r_1 & \cdots & g^r_{P_e} & 0 & 0 & \cdots & 0 \\ 0 & 1 & g^r_1 & \cdots & g^r_{P_e} & 0 & \cdots & 0 \\ \vdots & \vdots & \ddots & \ddots & & \ddots & \ddots & \vdots \\ 0 & 0 & \cdots & 0 & 1 & g^r_1 & \cdots & g^r_{P_e} \end{bmatrix}_{(N-P_e)\times N} \tag{51}$$

Equation (39), (48) and (49) give the Hermitian covariance matrix in (21) and it can be readily seen from (35) and (47) that $E\{\Delta\boldsymbol{\eta}\} = \mathbf{0}$ which implies that $E\{\hat{\boldsymbol{\eta}}\} = \boldsymbol{\eta}$. This completes the proof.

4. Results

4.1. FBEP's theoretical MSE vs. CR bound

We compare the theoretical MSEs of frequency and damping factor estimates of the FBEP method to the CR bounds to test the performance of the TLS-Prony method given in [30]. The test signal consists of one mode with a real pole (phase angle is zero) that is moving along the real axis from 0.1 to 10, with amplitude chosen to make the mode energy equal to unity. The noise is Gaussian with the total noise variance $2\sigma^2$ also set to unity. The prediction order is set to $N/3$, where the data length is N. The minimum MSE of the frequency estimates (Fig. 1) decreases as the data length increases from 2 to 100. Unlike the TLS-Prony method whose results significantly deviate from the corresponding CR bounds when the pole is outside the unit circle, the theoretical values for the FBEP method are symmetrical with respect to the unit circle and are close to the respective CR bounds. The theoretical MSEs curves of damping factor estimates and corresponding CR bounds are exactly the same as in Fig. 1 except that the values are scaled by $4\pi^2$.

4.2. Noise-free case

A 25-point data sequence $x(n)$ (one growing and one decaying mode) is generated as

$$x(n) = e^{(-0.1+j2\pi\cdot 0.42)n} + e^{(0.1+j2\pi\cdot 0.32)n}, \quad n = 0, 1, \ldots, 24 \tag{52}$$

The prediction order = 10, and the FBEP parameter estimates for the growing and decaying modes are compared with those obtained by Kumaresan and Tufts' method [22] in Table 1. The FBEP method gives accurate results for the two modes, whereas Kumaresan and Tufts' method fails to identify the growing mode and the amplitude and phase estimates of the decaying mode are incorrect.

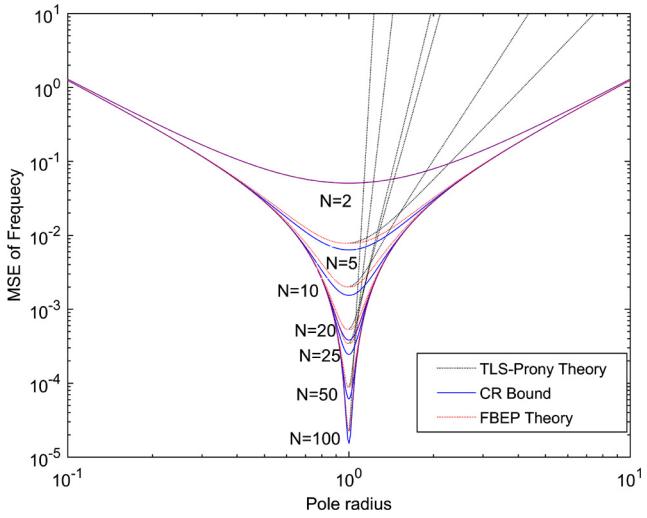

Fig. 1. Theoretical MSE of frequency estimate compared to corresponding CR bounds when the data length N is set to 2, 5, 10, 20, 25, 50 and 100 respectively. (For interpretation of the colors in the figure(s), the reader is referred to the web version of this article.)

Table 1
Prony analysis results of the FBEP method compared with Kumaresan and Tufts' method.

FBEP method			
Amplitude	Frequency	Damping factor	Phase
1.0000	0.4200	−0.1000	0.0000
1.0000	0.3200	0.1000	0.0000
Kumaresan and Tufts' method			
Amplitude	Frequency	Damping factor	Phase
1.3091	0.4200	−0.1000	−0.4434

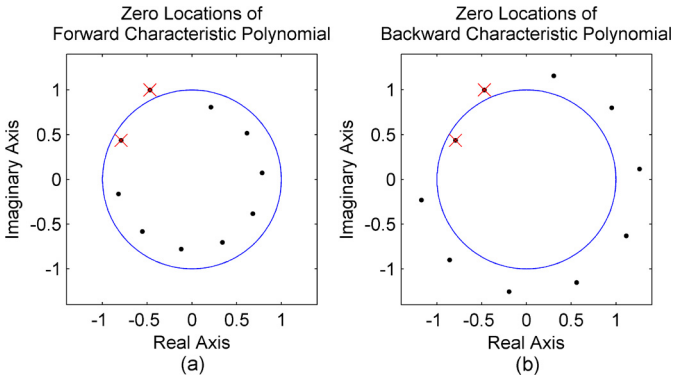

Fig. 2. Zero locations of forward and backward characteristic polynomials in noiseless case; with the true pole locations indicated by crosses.

The zero locations of the forward and backward characteristic polynomials of the FBEP method are shown in Fig. 2, where cross marks indicate the true pole locations. The signal zero locations are accurate estimates of the true poles and the extraneous zeros are approximately uniformly distributed around the unit circle.

4.3. Additive white Gaussian noise case

Zero-mean white Gaussian noise is added to $x(n)$ with different SNR $= 10\log(\frac{1}{2\sigma^2})$. The real and imaginary parts of the noise are uncorrelated with variance σ^2. 500 independent trials are implemented at each SNR level from 40 dB to 8 dB. The prediction order is $P_e = 10$, which is commonly used when comparing different methods [31,33]. The rank for the low rank approximation $= 2$

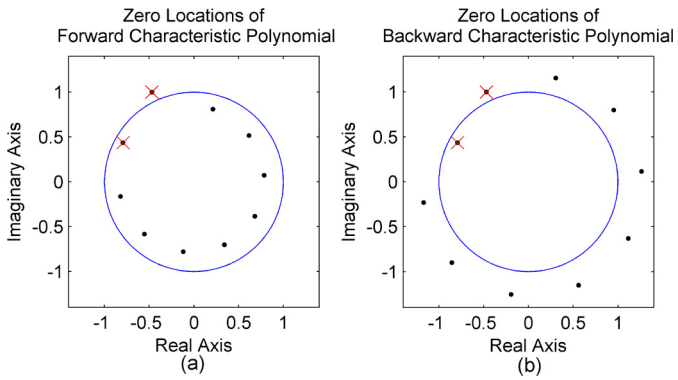

Fig. 3. Zero locations of forward and backward characteristic polynomials when SNR is 40 dB; with the true pole locations indicated by crosses.

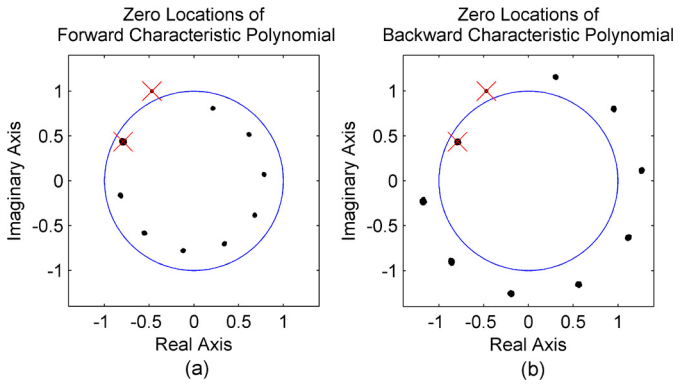

Fig. 4. Zero locations of forward and backward characteristic polynomials when SNR is 20 dB; the true pole locations are indicated by crosses.

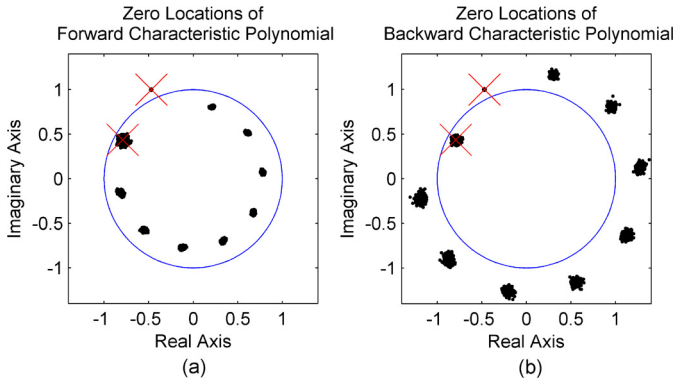

Fig. 5. Zero locations of forward and backward characteristic polynomials when SNR is 10 dB; the true pole locations are indicated by crosses.

when the TLS method is used to find the minimum norm solutions. Fig. 3, Fig. 4, and Fig. 5 show the superimposed zero locations of 500 trials with SNR = 40 dB, 20 dB and 10 dB respectively, and the sample means of the estimates of the four parameters are given in Table 2.

As the SNR decreases the accuracy of the mode estimates also decreases. The spread of the clusters becomes larger (increase in sample variance), and the noise has a greater impact on the decaying mode. The growing mode is dominant and is less affected by the noise.

The performance of FBEP is first compared to the TLS-Prony method with prediction order = 10 for both methods. Fig. 6 and Fig. 7 show the MSE of the frequency and damping factor estimates at different SNRs compared to the corresponding CR bounds. The MSEs for FBEP are close to the CR bounds for both decaying and

Table 2
Sample means of the estimates of the four parameters given by the FBEP method when SNR is 40, 20, 10 dB.

Decaying mode				
SNR	Amplitude	Frequency	Damping factor	Phase
40 dB	0.9999	0.4200	−0.1000	0.0002
20 dB	1.0026	0.4200	−0.1006	0.0001
10 dB	1.0197	0.4200	−0.1019	0.0013
Growing mode				
SNR	Amplitude	Frequency	Damping factor	Phase
40 dB	1.0001	0.3200	0.1000	0.0000
20 dB	1.0008	0.3200	0.1000	0.0002
10 dB	0.9981	0.3200	0.1001	−0.0008

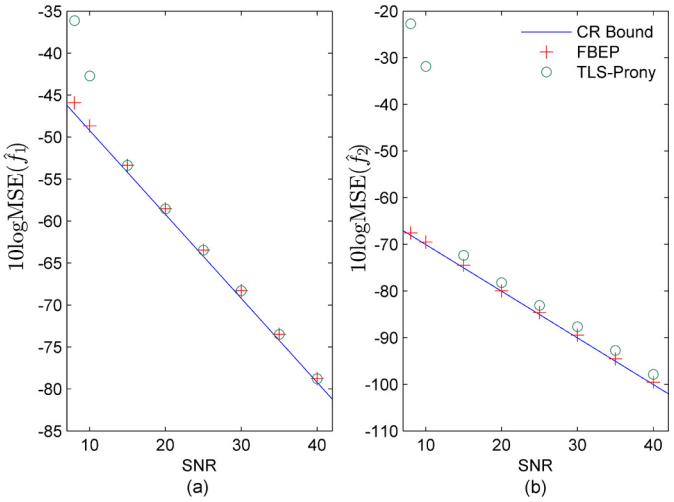

Fig. 6. MSE of frequency estimates given by FBEP and TLS-Prony at different SNR levels compared to corresponding CR bounds. $\hat{f}_1$ is the frequency estimate of the decaying mode and $\hat{f}_2$ is that of the growing mode.

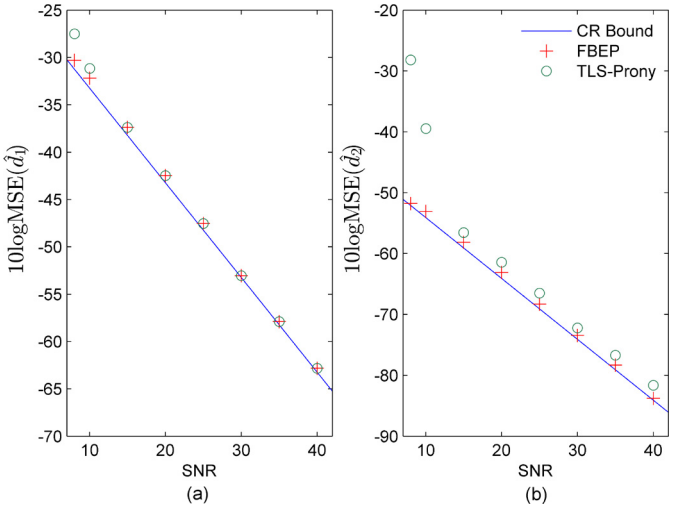

Fig. 7. MSE of damping factor estimates given by FBEP and TLS-Prony at different SNR levels compared to corresponding CR bounds. $\hat{d}_1$ is the damping factor estimate of the decaying mode and $\hat{d}_2$ is that of the growing mode.

growing modes. The TLS-Prony results deviate significantly from the CR bounds when the SNR = 10 dB and below and estimation of the growing mode is always worse than FBEP.

The performance (MSE) of FBEP as a polynomial method is compared to the subspace-based methods, specifically TLS-MP, TLS-ESPRIT and the MODE algorithm, in Fig. 8 and Fig. 9. Estimates given by the MODE algorithm are optimal with $d = 1$ and $m = 11$

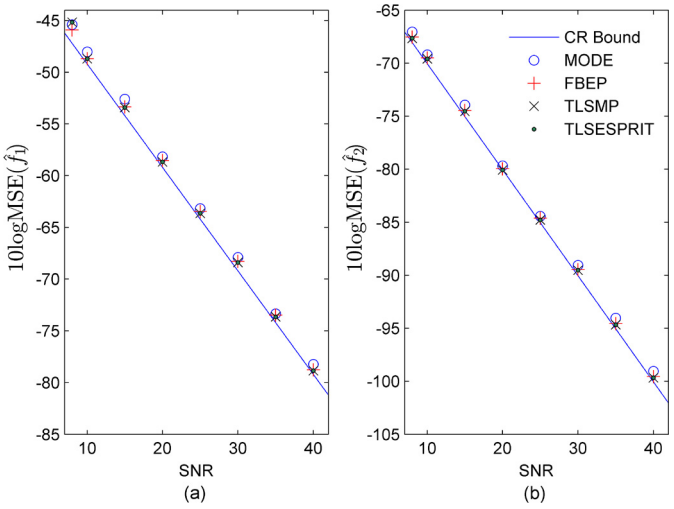

Fig. 8. MSE of frequency estimates given by FBEP and subspace-based methods at different SNR levels compared to corresponding CR bounds. $\hat{f}_1$ is the frequency estimate of the decaying mode and $\hat{f}_2$ is that of the growing mode.

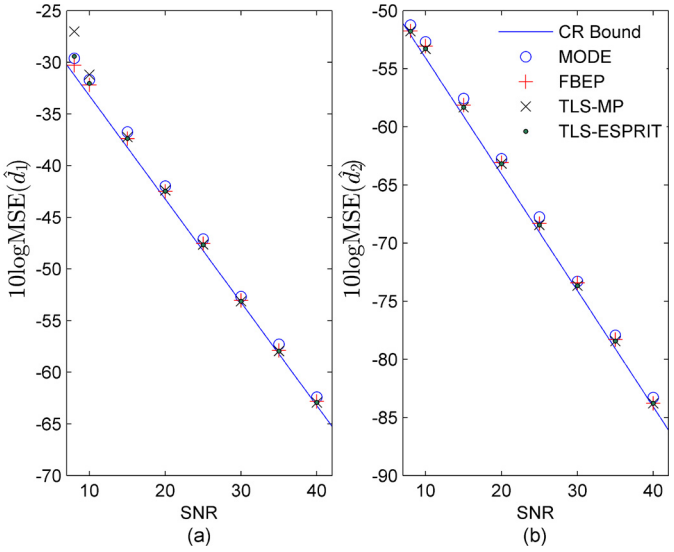

Fig. 9. MSE of damping factor estimates given by FBEP and subspace-based methods at different SNR levels compared to corresponding CR bounds. $\hat{d}_1$ is the damping factor estimate of the decaying mode and $\hat{d}_2$ is that of the growing mode.

[33]. The pencil parameter is 10 and the number of observations in one snapshot vector is also 10 for the TLS-ESPRIT method. The MODE algorithm performs better than TLS-Prony but is not as good as FBEP especially with relatively low SNR. The results corroborate that TLS-MP and TLS-ESPRIT provide good estimation results for high SNR levels. The performance of FBEP is comparable to these two methods at high SNR levels, where the MSEs of both frequency and damping factor estimates of the growing mode given by these three methods are close to the CR bounds at all tested SNRs. It is difficult to estimate a decaying mode especially the damping factor when a growing mode is present. For the tested SNRs, the FBEP method gives better estimation of the damping factor of the decaying mode than TLS-MP and TLS-ESPRIT when the SNR is 20 dB and below, with the exception that TLS-ESPRIT gives a negligibly lower MSE (0.02 dB lower) at the SNR level of 15 dB.

SVD is performed once in the FBEP method and it dominates the computational complexity of FBEP. Hence the computational complexity of FBEP is similar to that of SVD, i.e., $O(min((N - P_e)^2(P_e + 1), (N - P_e)(P_e + 1)^2)$. ESPRIT and Matrix Pencil are also non-iterative methods using SVD and they have the same com-

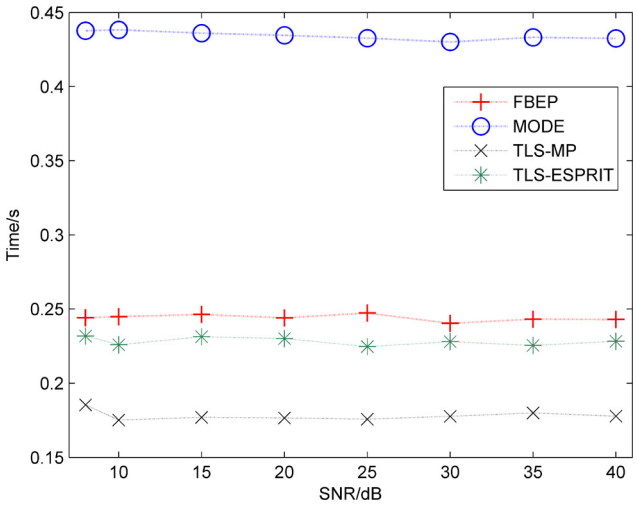

Fig. 10. Computational time of FBEP, MODE, TLS-MP, TLS-ESPRIT at different SNR levels.

putational complexity as FBEP. Fig. 10 displays the computational time of FBEP, TLS-MP, TLS-ESPRIT, and the MODE algorithm in Matlab R2015a running on Mac OSX with 2.4 GHz dual-core processor and 8 GB memory. The MODE algorithm has the longest computational time, which is more than a 78% increase of the other three methods on average. TLS-MP and TLS-ESPRIT are well-known for their computational efficiency and they give the shortest and the second shortest computational times respectively. The computational time of the FBEP method is close to that of TLS-ESPRIT, and its computational complexity is among the most efficient. The advantage of FBEP as a non-iterative method is supplemented by the comparison to the iterative optimization-based method ADMMHankel in Appendix A. The potential of FBEP to be applied to parameter estimation under pink noise is shown in Appendix B.

4.4. Performance when below the threshold SNR

For all SNR levels in the above experiments, both of the modes are identified by the FBEP method in each trial, however when the SNR is below 8 dB, identification of the two modes is not guaranteed; the decaying mode cannot always be found and the locations of some of the extraneous zeros no longer satisfy the properties given in the propositions due to the low SNR. This results in inaccurate detection (with fewer or greater number of modes) by the FBEP method and 8 dB is the threshold SNR. 500 independent trials are implemented when the SNR levels are below the threshold SNR, specifically at 6 dB, 5 dB and 4 dB, respectively. We organize the trials according to their FBEP results into three categories: those with a fewer number of modes, those with a greater number of modes, and those with the actual number of modes. The 0.32 Hz mode is always observed in all trials at all SNR levels. The zero locations for all 500 trials with 6 dB SNR are shown in Fig. 11.

Fig. 12 and Fig. 13 plot the zero locations at 6 dB SNR when the number of modes estimated is either one fewer or one greater than the actual, respectively.

In Fig. 14, the distribution of 500 independent trials for SNR levels at 6 dB, 5 dB and 4 dB is displayed and the results are compared to those where the pseudoinverse method is used to obtain the minimum norm solutions of the low rank approximation of the data matrix. No trials with more than two identified modes are found using the pseudoinverse method and the TLS method has results in all three categories. The performance of both methods deteriorates as the SNR decreases and the rate of deterioration of the pseudoinverse method is faster than that of the TLS method.

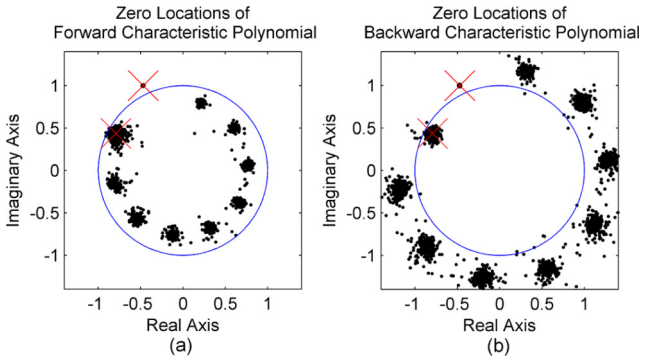

Fig. 11. Zero locations of forward and backward characteristic polynomials when SNR is 6 dB; the true pole locations are indicated by crosses.

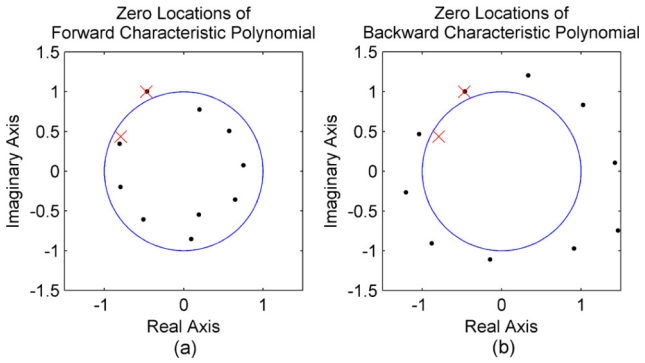

Fig. 12. Zero locations estimated when SNR is 6 dB, one mode fewer than actual; the true pole locations are indicated by crosses.

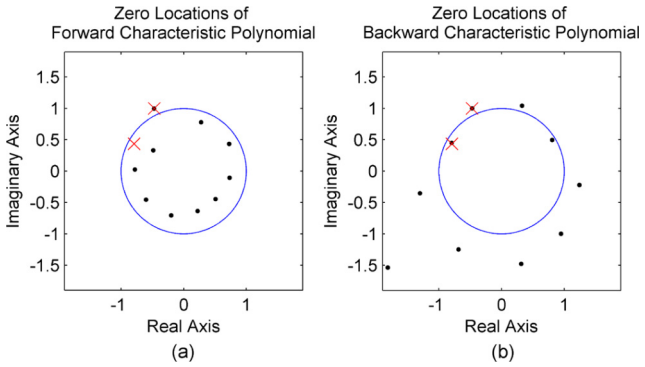

Fig. 13. Zero locations estimated when SNR is 6 dB, one mode greater than actual; the true pole locations are indicated by crosses.

Hence we conclude that the TLS method is more robust to decreasing SNR than the pseudoinverse method.

4.5. Four modes under white Gaussian noise

The performance of FBEP on multiple modes under white Gaussian noise is illustrated below. Two additional modes (one growing and one decaying) are added into the signal $x(n)$ so that there are four modes (two growing modes and two decaying modes) with different frequencies and damping factors. White Gaussian noise is added to $x_2(n)$ with SNRs in a similar way as in section 4.3.

$$x_2(n) = e^{(-0.1+j2\pi\cdot 0.42)n} + e^{(0.1+j2\pi\cdot 0.32)n} + e^{(-0.25+j2\pi\cdot 0.22)n} + e^{(0..25+j2\pi\cdot 0.35)n}, \quad n = 0, 1, \ldots, 24 \tag{53}$$

As can be seen from Figs. 15–17, FBEP can accurately identify the four modes under high SNRs, and as the SNR decreases we ob-

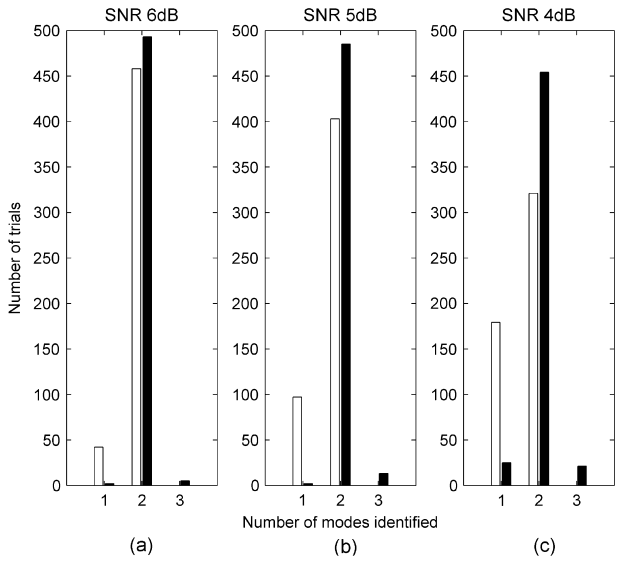

Fig. 14. Distribution of 500 independent trials into three categories when SNR is 6 dB, 5 dB, 4 dB respectively; white bars correspond to the pseudoinverse method and black bars correspond to the TLS method.

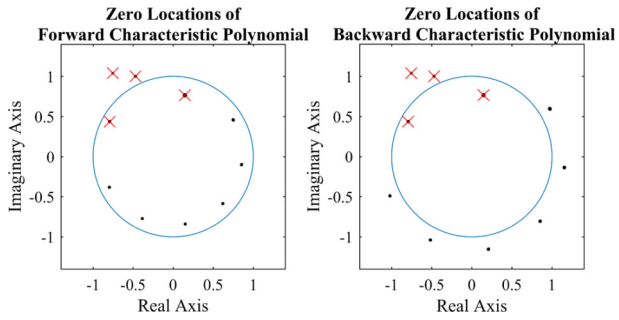

Fig. 15. Zero locations of forward and backward characteristic polynomials when SNR is 40 dB; the true pole locations are indicated by crosses.

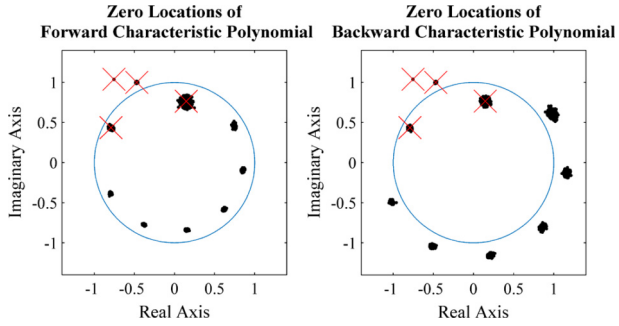

Fig. 16. Zero locations of forward and backward characteristic polynomials when SNR is 20 dB; the true pole locations are indicated by crosses.

serve similar phenomena as in the two-mode case. The noise has greater impact on the decaying modes than the growing modes. This is because the energy of growing modes increases with time and the energy of the decaying modes decreases with time. On the other hand for modes where the damping factors have the same sign (both growing and both decaying), the modes with the smaller damping factors are more affected by the noise resulting in a larger spread of the clusters because they have relatively smaller energy.

5. Conclusion

In this paper we have developed the FBEP method that uses a new strategy to identify the true poles. FBEP provides accurate

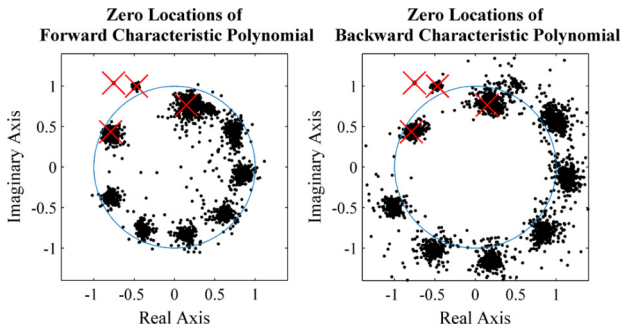

Fig. 17. Zero locations of forward and backward characteristic polynomials when SNR is 10 dB; the true pole locations are indicated by crosses.

estimation results as well as computational efficiency regardless of the existence of decaying or growing modes when the signal is corrupted significantly by noise. We have also shown that the FBEP method is superior to the TLS-Prony method in terms of both statistical analysis and simulation results. As a polynomial method, FBEP provides new insight into the estimation performance of polynomial methods and evidence to counter the belief that the estimation performance of these methods is much worse than the subspace-based methods under considerable noise. Specifically the FBEP method provides better results than the MODE algorithm and gives comparable performance to TLS-MP and TLS-ESPRIT while offering good estimation accuracy of the damping factor of the decaying mode under moderately low SNRs. The computational complexity of the FBEP method is among the most efficient. FBEP also gives better performance than the optimization-based method ADMMHankel by providing better estimation accuracy under low SNRs with significantly less computational time. Preliminary analysis shows the potential of FBEP for parameter estimation under pink noise.

The ability to identify the true modes under low SNRs with small computational cost makes FBEP suitable to be used effectively in practical applications. Future research could include applying FBEP for on-line stability analysis of large-scale power systems using PMU data and using FBEP for parameter estimation in biological systems with pink noise.

Conflict of interest statement

There is no conflict of interest.

Appendix A

We have compared the performance of the ADMMHankel method with that of the FBEP method and TLS-ESPRIT method using the same experiments as given previously on a data sequence of 25 samples with different SNR. The tuning parameters of the ADMMHankel method are set to the same as given in [36], i.e., $\rho = 0.025$ and $niter = 200$.

As can be seen from Fig. 18 and Fig. 19, the frequency and damping factor estimates given by ADMMHankel deviate significantly from the corresponding Cramer–Rao bounds at SNR of 15 dB and below for the decaying mode and at 10 dB and below for the growing mode, and its performance at these SNR levels is not comparable to that of FBEP and TLS-ESPRIT. Under high SNR ADMMHankel achieves slightly better results than FBEP and TLS-ESPRIT due to the iterative use of the low-rank approximation and the formation of the Hankel matrix. This idea of iteratively performing low-rank approximation and Hankel matrix forming (also known as the low-rank Hankel matrix approximation) was originally proposed by the authors of [45] in 1997, where the low-rank Hankel matrix approximation was incorporated into the Kumaresan and Tufts' method (a Prony variant) to provide improved esti-

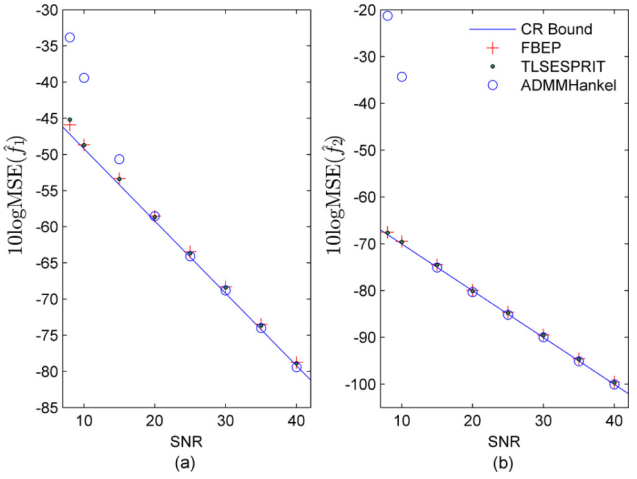

Fig. 18. MSE of frequency estimates given by FBEP, TLS-ESPRIT and ADMMHankel at different SNR levels compared to corresponding CR bounds. $\hat{f}_1$ is the frequency estimate of the decaying mode and $\hat{f}_2$ is that of the growing mode.

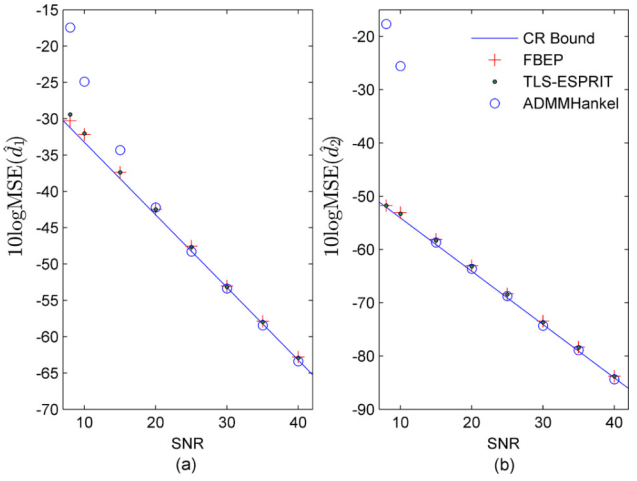

Fig. 19. MSE of damping factor estimates given by FBEP, TLS-ESPRIT and ADMMHankel at different SNR levels compared to corresponding CR bounds. $\hat{d}_1$ is the frequency estimate of the decaying mode and $\hat{d}_2$ is that of the growing mode.

mation accuracy for damped exponential signals consisting of decaying modes only. This technique can also be readily incorporated into the FBEP and TLS-ESPRIT methods to achieve similar results to those of ADMMHankel under high SNR and even better results under low SNR while using only a few iterations (2 iterations in [45]).

The computational time of ADMMHankel for each experiment is shown in Fig. 20 with the average computational time of 568.8845 s whereas the computational time of FBEP and TLS-ESPRIT is less than 0.25 s as shown in Fig. 10. All experiments are tested using Matlab R2015a running on Mac OSX with 2.4 GHz dual-core processor and 8 GB memory on the same computer. The optimization-based method ADMMHankel is not suitable for real-time applications due to its computational complexity and long time as compared to the non-iterative FBEP and TLS-ESPRIT methods.

Appendix B

The FBEP method is proposed for parameter estimation under additive white Gaussian noise, a common noise model that is used in many applications. It is also interesting to see the performance of FBEP under non-white noise, such as pink noise. Pink $(1/f)$ noise is a common type of noise that is observed in biological systems. Unlike white noise that has a flat power spectrum with

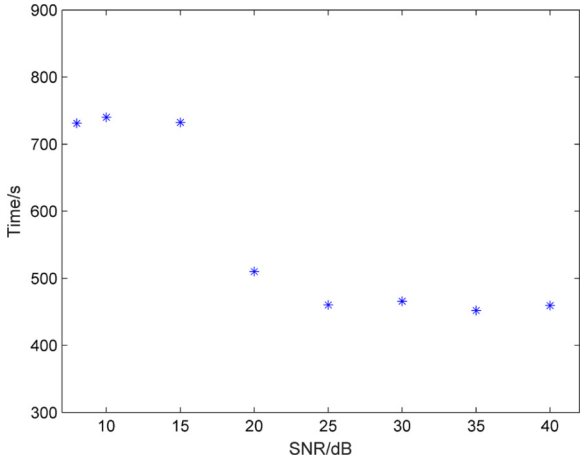

Fig. 20. Computational time of ADMMHankel at different SNR levels.

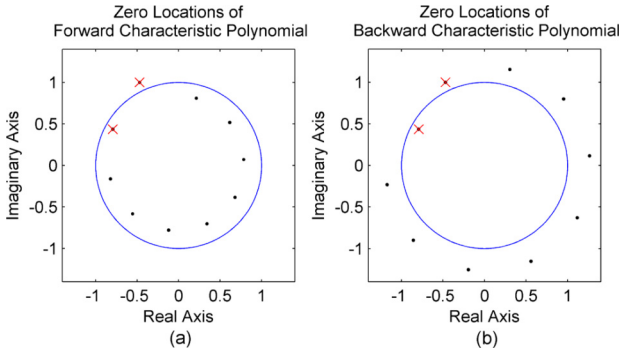

Fig. 21. Zero locations of forward and backward characteristic polynomials when SNR is 40 dB under pink noise; the true pole locations are indicated by crosses.

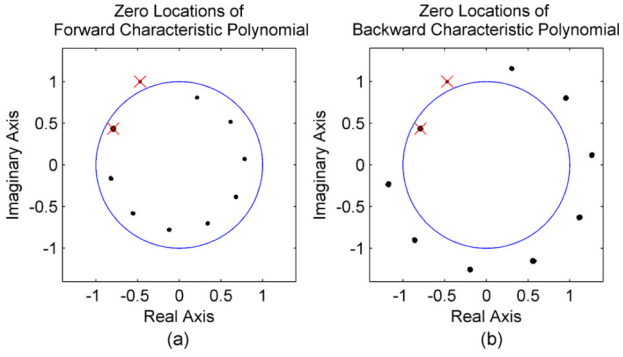

Fig. 22. Zero locations of forward and backward characteristic polynomials when SNR is 20 dB under pink noise; the true pole locations are indicated by crosses.

constant power across all frequencies, the frequency spectrum of pink noise is inversely proportional to the frequency of the signal and each octave carries an equal amount of noise energy.

We perform an initial study on the performance of FBEP by adding pink noise to the signal containing two modes given in section 4.2 with the same definition of SNR. 500 independent trials are implemented at each SNR level from 40 dB to 8 dB. As shown in Fig. 21 to Fig. 23 the spread of the clusters becomes larger as SNR decreases and the pink noise has greater impact on the decaying mode than the growing mode. The performance of FBEP and TLS-ESPRIT are similar as shown in Fig. 24 and Fig. 25. CR bounds of white noise are provided as a reference to show the performance of FBEP and TLS-ESPRIT as the noise changes from white to pink.

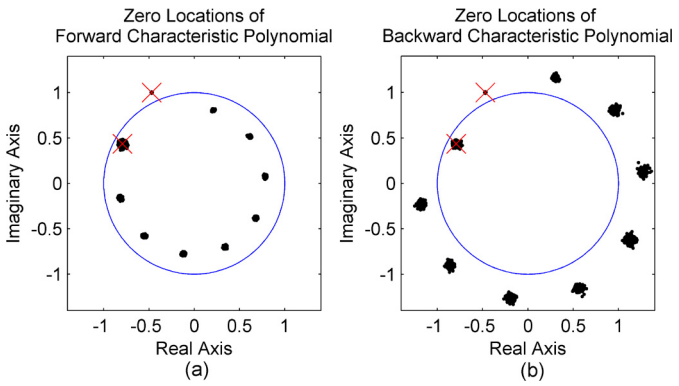

Fig. 23. Zero locations of forward and backward characteristic polynomials when SNR is 10 dB under pink noise; the true pole locations are indicated by crosses.

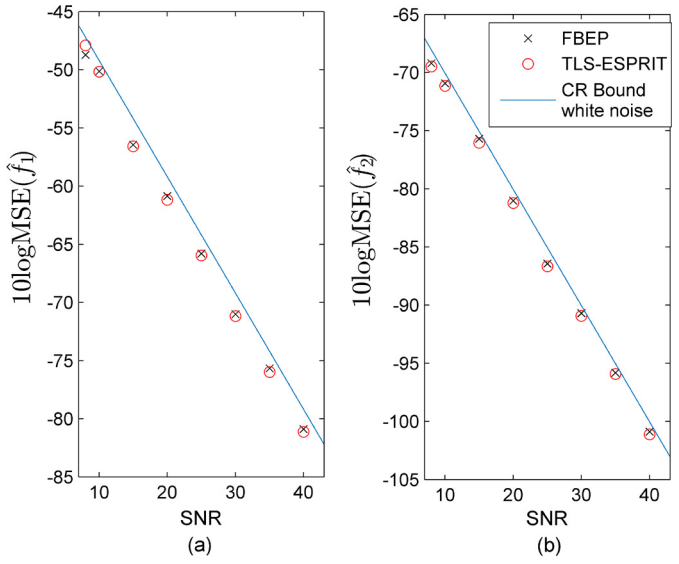

Fig. 24. MSE of frequency estimates given by FBEP, TLS-ESPRIT at different SNR levels compared to corresponding white noise CR bounds. $\hat{f}_1$ is the frequency estimate of the decaying mode and $\hat{f}_2$ is that of the growing mode.

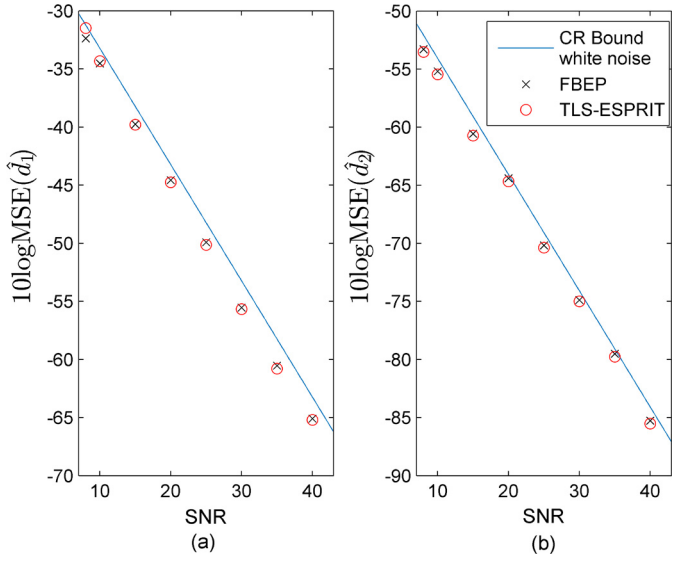

Fig. 25. MSE of damping factor estimates given by FBEP, TLS-ESPRIT at different SNR levels compared to corresponding white noise CR bounds. $\hat{d}_1$ is the frequency estimate of the decaying mode and $\hat{d}_2$ is that of the growing mode.

References

[1] N. Soon-Ryul, K. Sang-Hee, P. Jong-Keun, An analytic method for measuring accurate fundamental frequency components, IEEE Trans. Power Deliv. 17 (2002) 405–411.
[2] J.A. de la O Serna, Synchrophasor estimation using Prony's method, IEEE Trans. Instrum. Meas. 62 (2013) 2119–2128.
[3] W. Juanjuan, F. Chuang, Z. Yao, Design of WAMS-based multiple HVDC damping control system, IEEE Trans. Smart Grid 2 (2011) 363–374.
[4] A. Hasanovic, A. Feliachi, A. Hasanovic, N.B. Bhatt, A.G. DeGroff, Practical robust PSS design through identification of low-order transfer functions, IEEE Trans. Power Syst. 19 (2004) 1492–1500.
[5] D. Potts, M. Tasche, Parameter estimation for exponential sums by approximate Prony method, Signal Process. 90 (2010) 1631–1642.
[6] M. Roy, S. Barman, Novel approach to power spectrum estimation of DNA sequence by Prony's method, in: International Conference on Communications, Devices and Intelligent Systems, CODIS, 2012, pp. 314–317.
[7] S. Dencks, G. Schmitz, Estimation of multipath transmission parameters for quantitative ultrasound measurements of bone, IEEE Trans. Ultrason. Ferroelectr. Freq. Control 60 (2013) 1884–1895.
[8] H. Baali, R. Akmeliawati, M.J.E. Salami, A. Khorshidtalab, E. Lim, ECG parametric modeling based on signal dependent orthogonal transform, IEEE Signal Process. Lett. 21 (2014) 1293–1297.
[9] D.V. Lakshmi, G. Gayatri, Application of speech signals to deterministic signal modeling techniques, Int. J. Comput. Appl. 100 (2014).
[10] H. Heidar, A. Tavakoli, Highly dispersive scattering centre analysis using an enhanced parametric model, IET Radar Sonar Navig. 5 (2011) 895–901.
[11] L. Marple, T. Brotherton, Detection and classification of short duration underwater acoustic signals by Prony's method, in: International Conference on Acoustics, Speech, and Signal Processing, ICASSP-91, vol. 2, 1991, pp. 1309–1312.
[12] S.L. Marple, Digital Spectral Analysis: With Applications, Prentice-Hall, Englewood Cliffs, N.J, 1987.
[13] R.W. Kulp, An optimum sampling procedure for use with the Prony method, IEEE Trans. Electromagn. Compat. EMC-23 (1981) 67–71.
[14] J.C.H. Peng, N.K.C. Nair, Adaptive sampling scheme for monitoring oscillations using Prony analysis, IET Gener. Transm. Distrib. 3 (2009) 1052–1060.
[15] J.H. Lee, H.T. Kim, Selection of sampling interval for least squares Prony method, Electron. Lett. 41 (2005) 47.
[16] N. Zhou, J. Pierre, D. Trudnowski, Some considerations in using Prony analysis to estimate electromechanical modes, in: IEEE Power & Energy Society General Meeting, 2013, pp. 1–5.
[17] P. Tripath, S.C. Srivastava, S.N. Singh, An improved Prony method for identifying low frequency oscillations using synchro-phasor measurements, in: International Conference on Power Systems, ICPS'09, 2009, pp. 1–5.
[18] R. Kumaresan, Y. Feng, FIR prefiltering improves Prony's method, IEEE Trans. Signal Process. 39 (1991) 736–741.
[19] R. Zivanovic, P. Schegner, Pre-filtering improves Prony analysis of disturbance records, in: Eighth IEE International Conference on Developments in Power System Protection, vol. 2, 2004, pp. 780–783.
[20] F.F. Costa, A.J.M. Cardoso, Harmonic and interharmonic identification based on improved Prony's method, in: 32nd Annual Conference on IEEE Industrial Electronics, IECON 2006, 2006, pp. 1047–1052.
[21] D.W. Tufts, R. Kumaresan, Singular value decomposition and improved frequency estimation using linear prediction, IEEE Trans. Acoust. Speech Signal Process. 30 (1982) 671–675.
[22] R. Kumaresan, D.W. Tufts, Estimating the parameters of exponentially damped sinusoids and pole-zero modeling in noise, IEEE Trans. Acoust. Speech Signal Process. 30 (1982) 833–840.
[23] P. Kundur, Power System Stability and Control, McGraw-Hill, New York, 1994.
[24] J.L. Rueda, C.A. Juarez, I. Erlich, Wavelet-based analysis of power system low-frequency electromechanical oscillations, IEEE Trans. Power Syst. 26 (2011) 1733–1743.
[25] A.R. Borden, B.C. Lesieutre, Variable projection method for power system modal identification, IEEE Trans. Power Syst. 29 (2014) 2613–2620.
[26] R. Carriere, R.L. Moses, High resolution radar target modeling using a modified Prony estimator, IEEE Trans. Antennas Propag. 40 (1992) 13–18.
[27] R. Kumaresan, D.W. Tufts, L.L. Scharf, A Prony method for noisy data: choosing the signal components and selecting the order in exponential signal models, Proc. IEEE 72 (1984) 230–233.
[28] D.J. Trudnowski, Order reduction of large-scale linear oscillatory system models, IEEE Trans. Power Syst. 9 (1994) 451–458.
[29] N. Zhou, J.W. Pierre, D. Trudnowski, A stepwise regression method for estimating dominant electromechanical modes, IEEE Trans. Power Syst. 27 (2012) 1051–1059.
[30] W.M. Steedly, C.-H.J. Ying, R.L. Moses, Statistical analysis of TLS-based Prony techniques, Automatica 30 (1994) 115–129.
[31] T.K. Sarkar, O. Pereira, Using the matrix pencil method to estimate the parameters of a sum of complex exponentials, IEEE Antennas Propag. Mag. 37 (1995) 48–55.
[32] R. Roy, T. Kailath, ESPRIT – estimation of signal parameters via rotational invariance techniques, IEEE Trans. Acoust. Speech Signal Process. 37 (1989) 984–995.

[33] M. Cedervall, P. Stoica, R. Moses, u. Uppsala, MODE-type algorithm for estimating damped, undamped, or explosive modes, Circuits Syst. Signal Process. 16 (1997) 349–362.
[34] D. Potts, M. Tasche, Parameter estimation for nonincreasing exponential sums by Prony-like methods, Linear Algebra Appl. 439 (2013) 1024–1039.
[35] J. Swärd, S.I. Adalbjörnsson, A. Jakobsson, High resolution sparse estimation of exponentially decaying signals, in: IEEE International Conference on Acoustics, Speech and Signal Processing, ICASSP, 2014, pp. 7203–7207.
[36] F. Andersson, M. Carlsson, J.-Y. Tourneret, H. Wendt, A new frequency estimation method for equally and unequally spaced data, IEEE Trans. Signal Process. 62 (2014) 5761–5774.
[37] R. Kumaresan, On the zeros of the linear prediction-error filter for deterministic signals, IEEE Trans. Acoust. Speech Signal Process. 31 (1983) 217–220.
[38] S. Zhao, K.A. Loparo, Forward and backward extended prony (FBEP) method for power system small-signal stability analysis, IEEE Trans. Power Syst. 32 (2017) 3618–3626.
[39] P. Stoica, R.L. Moses, Introduction to Spectral Analysis, Prentice Hall, Upper Saddle River, N.J., 1997.
[40] M.D. Rahman, Y. Kai-Bor, Total least squares approach for frequency estimation using linear prediction, IEEE Trans. Acoust. Speech Signal Process. 35 (1987) 1440–1454.
[41] J.A. Cadzow, Spectral estimation: an overdetermined rational model equation approach, Proc. IEEE 70 (1982) 907–939.
[42] S. Zhao, Forward and Backward Extended Prony (FBEP) Method with Applications to Power System Small-Signal Stability, Ph.D dissertation, Case Western Reserve University, 2017.
[43] W.M. Steedly, C.H.J. Ying, R.L. Moses, A modified TLS-Prony method using data decimation, IEEE Trans. Signal Process. 42 (1994) 2292–2303.
[44] P. Stoica, A. Nehorai, MUSIC, maximum likelihood, and Cramer–Rao bound, IEEE Trans. Acoust. Speech Signal Process. 37 (1989) 720–741.
[45] L. Ye, K.J.R. Liu, J. Razavilar, A parameter estimation scheme for damped sinusoidal signals based on low-rank Hankel approximation, IEEE Trans. Signal Process. 45 (1997) 481–486.

Shuang Zhao received the B.E. degree in Automation from Nanchang University in 2007 and the Ph.D. degree in Systems and Control Engineering from Case Western Reserve University in 2017. Her research interest covers statistical signal processing, parameter estimation and their applications in electric power systems.

Kenneth A. Loparo is the Arthur L. Parker Professor in the EECS Department and Faculty Director of the Institute for Smart, Secure and Connected Systems (ISSACS) at Case Western Reserve University. Dr. Loparo's research interests include stability and control of nonlinear systems with applications to large-scale electric power systems and nonlinear filtering with applications to monitoring, fault detection, diagnosis and reconfigurable control in engineered and biological systems. Dr. Loparo is a Life Fellow of the IEEE and Fellow of AIMBE.